Acta Cryst A FOUNDATIONS ADVANCES
ISSN 2053-2733

Neutron interferometric measurement and calculations of a phase shift induced by Laue transmission

T. Potocar,[a]* M. Zawisky,[a] H. Lemmel,[a,b] J. Springer[a] and M. Suda[a,c]

[a]Vienna University of Technology, Institute of Atomic and Subatomic Physics, A-1020 Vienna, Austria, [b]Institut Laue–Langevin, F-38000 Grenoble, France, and [c]Austrian Institute of Technology – AIT, A-1220 Vienna, Austria. *Correspondence e-mail: tpotocar@ati.ac.at

Received 28 October 2014
Accepted 23 June 2015

Edited by D. A. Keen, STFC Rutherford Appleton Laboratory, UK

Keywords: Neutron interferometry; perfect crystal interferometer; large-area interferometer; dynamical diffraction; beam deflection; neutron–electron scattering lengths.

This study investigates the phase shift induced by Laue transmission in a perfect Si crystal blade in unprecedented detail. This 'Laue phase' was measured at two wavelengths in the vicinity of the Bragg condition within a neutron interferometer. In particular, the sensitivity of the Laue phase to the alignment of the monochromator and interferometer (rocking angle) and beam divergence has been verified. However, the influence of fundamental quantities, such as the neutron–electron scattering length, on the Laue phase is rather small. The fascinating steep phase slope of 5.5° [(220) Bragg peak] and 11.5° [(440) Bragg peak] per 0.001 arcsec deviation from the Bragg angle has been achieved. The results are analysed using an upgraded simulation tool.

1. Introduction

Neutron interferometers (IFMs) are used to determine quantum mechanical effects on the neutron wave. As for X-ray interferometers, the interaction of the neutron wave within the IFM is described by the dynamical theory of diffraction (Authier, 2006). Such interferometers are built in the form of a Mach–Zehnder IFM and consist of one large silicon crystal. Here we use such a setup to measure the phase of a perfect Si crystal sample close to the Bragg position. The first measurements of this 'Laue phase' were presented in Springer *et al.* (2010). They offer in principle the possibility of extracting fundamental quantities such as the neutron–electron scattering length, gravitational short-range interactions and the Debye–Waller factor (Ioffe & Vrana, 2002; Wiedtfeldt *et al.*, 2006; Greene & Gudkov, 2007). For this purpose, it is necessary to improve the accuracy of the phase measurement – and consider all systematic phase effects in the analysis.

Our previous article (Springer *et al.*, 2010) left several open questions concerning the influence of different parameters; therefore this article presents a more systematic investigation of the Laue phase. As experimental improvements, an aluminium box for temperature stabilization of the interferometer has been installed, the number of measurements has been increased and the angular range of the beam deflection has been further enlarged.

Previous publications related to the Laue phase are Graeff *et al.* (1978), Rauch (1989), Hirano & Momose (1996), Ioffe & Vrana (2002), Authier (2006), Lemmel (2007), Springer *et al.* (2010), Lemmel (2013*b*). §2 explains the experimental setup, where a large six-blade Si perfect crystal interferometer with precisely oriented lattice planes was used. All the measure-

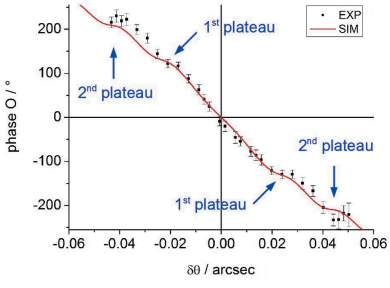

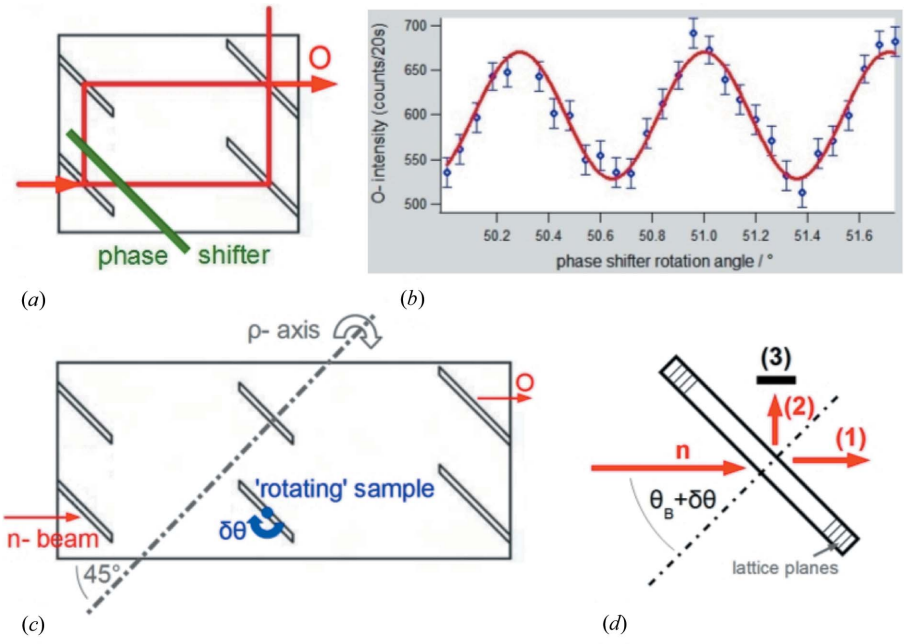

Figure 1
(*a*) Sketch of a Mach–Zehnder interferometer with a phase shifter intersecting the two beam paths. (*b*) Typical interferogram in the output *O*: the intensity is recorded *versus* the phase shifter rotation. The phase and fringe visibility are derived from this sinusoidal intensity modulation. (*c*) Neutron interferometer with rotating sample. (*d*) Top view of the sample with the $\delta\theta$ angle: (1) transmitted beam, (2) diffracted beam, (3) beam stopper.

ments were performed at instrument S18 at the ILL Grenoble. In §3, we discuss important parameters to be considered in precision experiments. These parameters are the type of monochromator, its mosaicity, rocking position (alignment angle between monochromator and interferometer) and IFM geometry. We compare the experiment with theoretical calculations of the Laue phase. All these calculations are performed using an upgraded simulation tool; a detailed description of the software *IFMSIM* is provided in Lemmel (2013*a*).

2. Measurement of the Laue phase

An analytical expression of this phase is given in equation (1) for a monochromatic plane wave in a perfect crystal blade of thickness D (Springer *et al.*, 2010; Zawisky, Springer & Lemmel, 2010):

$$\varphi_{\rm Laue}(y) = \varphi_{\rm Laue}(0) - A_H \times y + \arctan\left\{\frac{y}{(1+y^2)^{1/2}}\tan\left[A_H(1+y^2)^{1/2}\right]\right\} \quad (1)$$

with

$$y = -\delta\theta \times \sin(2\theta_{\rm B}) \times E/|V_{hkl}|$$
$$A_H = \pi D/\Delta_H$$
$$\Delta_H = \frac{2\pi\cos\theta_{\rm B}\times E}{k\times|V_{hkl}|} = \frac{\pi n_r}{2d_{\rm L}Nb_{\rm atom}(q)\exp[-W(q)]\tan\theta_{\rm B}}. \quad (2)$$

Here, $\delta\theta$ is the beam deviation from the Bragg angle $\theta_{\rm B} = 45°$, E is the neutron energy, $|V_{hkl}|$ is the crystal potential (Rauch & Petrascheck, 1974) and Δ_H denotes the *Pendellösung* length, with n_r representing the order of the Bragg peak, $d_{\rm L}$ representing the lattice spacing, $N = 4.9939678 \times 10^{22}$ cm^{-3} representing the atomic density for Si, $b_{\rm atom}$ representing the atomic scattering length and W the Debye–Waller factor. The momentum transfer is given by $q = 2\pi n_r/d_{\rm L}$. According to the dynamical theory of diffraction, the *Pendellösung* length describes the period length of the wavefield oscillation within the crystal (Shull, 1968).

In general, a phase within an interferometer is measured by recording the output intensity in the *O* detector *versus* the rotation angle of an auxiliary phase shifter. In our case we use a 3 mm-thick Si phase shifter after blade 1. A Mach–Zehnder-type interferometer together with the sinusoidal interferogram is depicted in Figs. 1(*a*), 1(*b*).

The principle of measuring the Laue phase is illustrated in Figs. 1(*c*), 1(*d*) with a rotating sample, where the rotation angle is $\delta\theta$. For every $\delta\theta$ a complete interferogram is taken. The phase shift of the interferogram due to the small sample rotation is the 'Laue phase'. The blade in the second beam compensates for the refractive phase of the sample.

However, in the experiment, the sample is fixed, and a pair of aluminium prisms deflect the beam in front and behind the IFM blade (Fig. 2). This beam deflection is controlled *via* a

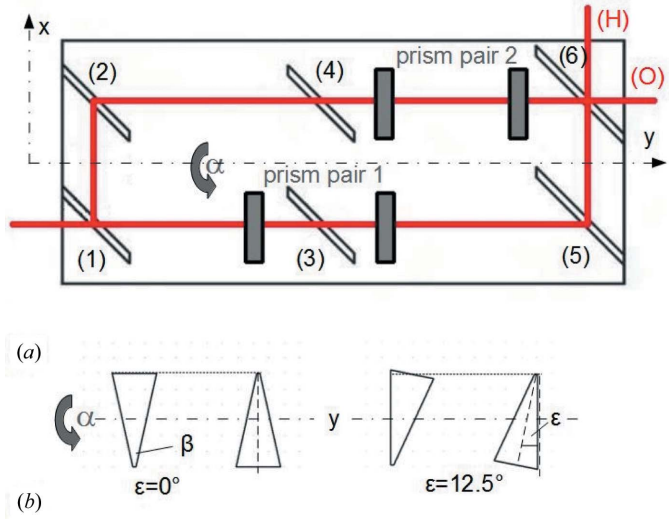

Figure 2
(*a*) Top view of the experiment. The incident wave is split at blade (1) and passes through the sample blades (3), (4) and prisms, which rotate around the *y* axis (α). After recombination in blade (6), the interferogram in the transmitted beam (*O*) is recorded. (*b*) Prism side view and mounting angle $\varepsilon = 12.5°$ ($\beta = 25°$).

rotation α of the prisms. The correlation between the beam deflection and the rotation angle α of the prisms is given in equation (3) (Ioffe & Vrana, 2002):

$$\delta\theta = \delta \sin\alpha \tag{3}$$

$$\delta = 2(1-n)\frac{\sin\beta}{\cos\beta + \cos 2\varepsilon}$$
$$n = 1 - \frac{\lambda^2 N b_{\rm N}}{2\pi}. \tag{4}$$

The prism angle β is 25° and ε, the deviation of the symmetric prism mounting, is then 12.5° (Fig. 2); λ is the wavelength, and the nuclear scattering density $Nb_{\rm N} = 2.08\ {\rm cm}^{-2}$ (Rauch & Werner, 2002). In our upgraded setup, a range of $\alpha = \pm 15°$ is experimentally accessible, which accounts for the (220) case to $\delta\theta = \pm 0.06$ arcsec and ± 0.015 arcsec for (440).

Wavelength selection. In order to compare the Laue phase at two wavelengths, two Bragg peaks from the silicon monochromator have been chosen. To separate the used Bragg peaks (220), (440) from each other, six $\beta_i = 140°$ silicon prisms were arranged in front of the interferometer. From equation (4) (Zawisky, Springer, Farthofer & Kuetgens, 2010), using the nuclear scattering length $b_{\rm N} = 4.1507\ (2)$ fm, the following total beam deflection is derived:

$$\delta(\lambda) = \lambda^2 \sum_{i=1}^{6} \frac{N b_{\rm N}}{\pi} \tan\frac{\beta_i}{2}. \tag{5}$$

The separation between the (220) and (440) Bragg peaks amounts to 13″. It can be determined by performing a rocking curve, where the rocking angle describes the rotation of the IFM in the x–y plane relative to the incident beam (Fig. 3). By inserting a diffraction grating ($g = 16$ µm) in front of the interferometer, the wavelengths in the Bragg peaks can be determined (Bergmann & Schaefer, 1993):

$$\lambda = g\frac{\sin\varphi_{n'}}{n'}. \tag{6}$$

The diffraction maxima behind the grating are located at the angle $\varphi_{n'}$, where n' is the diffraction order. For the (440) case, we derive a wavelength of (1.35 ± 0.04) Å; the (220) wavelength is twice this value: (2.71 ± 0.04) Å.

2.1. Measurements in the (220) case

With the above-described Si prisms we are now able to measure the Laue phase with $\lambda = 2.71$ and 1.35 Å separately. In the calculations we use the real geometry of the interferometer, the maximal intensity of the rocking peaks (rocking position 0) and the Bragg monochromator function with Darwin width equal to 1. The neutron beam is calculated as a coherent superposition of many plane waves (spherical wave), while equation (1) describes the Laue phase with only a single plane wave. Important for the understanding of the phase and contrast behaviour is the averaging over all plane-wave components. Therefore the phase slope becomes about 1/3 smaller than for a single plane wave. Fig. 4 shows the (220) Laue phase for a wide range of beam deflections ($\delta\theta = \pm 0.06''$) in front of blade 3. The slope of the phase curve near the Bragg position amounts to 5.5°/0.001 arcsec and fits very well with the calculations.

Two non-linearities in the phase curve (‘*Pendellösung* plateaus’) can be identified at each side near the Bragg position. These structures are related to oscillations resulting from the interference of two internal wavefields with slightly different wavevectors (Shull, 1968). They appear exactly at the minima of the transmitted intensity and are described by the arcus tangents in equation (1). The phase plateaus are at the poles of the tangents; small changes in its argument $A_H(1+y^2)^{1/2} = (2n+1)\pi/2$ show an enhanced sensitivity to the phase.

Besides the phase, the fringe visibility (contrast) of the interferograms (Fig. 1) is also considered. The diminishing of

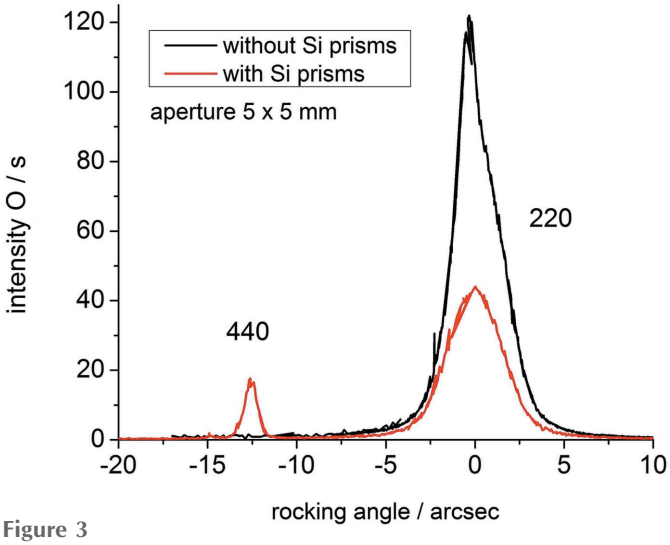

Figure 3
Separation of the (220) and (440) Bragg peaks by the use of Si prisms in front of the interferometer. The phase measurements will be performed exactly at each peak maximum.

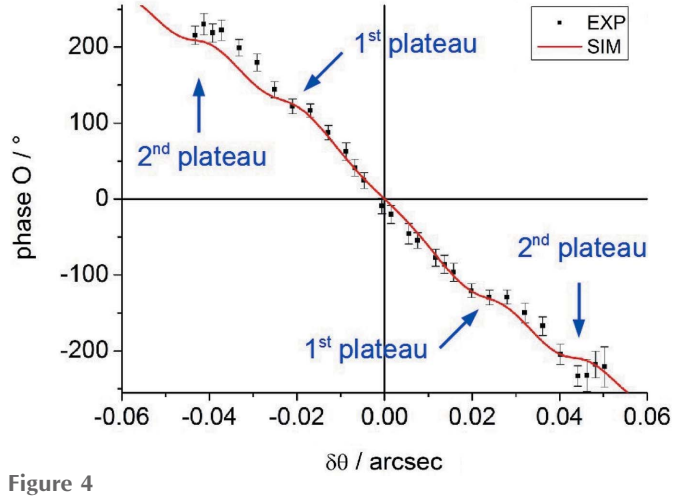

Figure 4
Measured (EXP) and calculated (SIM) Laue phase for the (220) case. The marked *Pendellösung* plateaus are regions with increased sensitivity to parameter A_H.

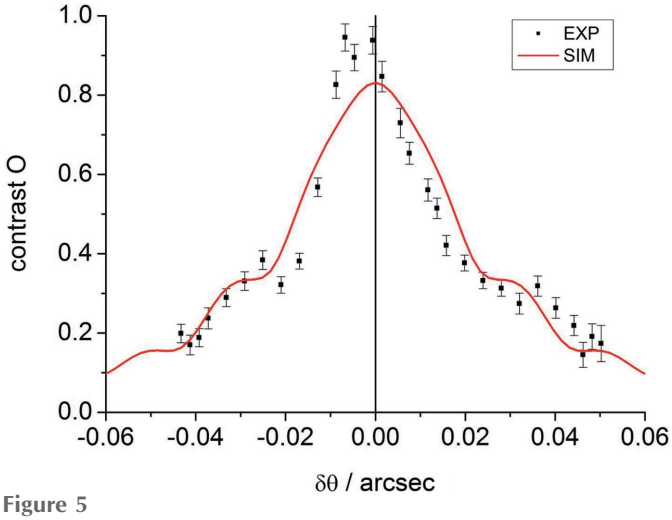

Figure 5
Measured and calculated contrast for the (220) case. The contrast decreases with increasing beam deflection.

the interference pattern with increasing $\delta\theta$ is shown in Fig. 5. Due to the low contrast, measurements at $\delta\theta > 0.02$ arcsec become increasingly challenging. The contrast reduction is mainly caused by a distinct phase distribution within the divergence of the incoming beam. Asymmetric beam-path intensities reduce the fringe visibility as well. This asymmetry results from the blade 3 rotation during the measurement. The *Pendellösung* plateaus are visible in the contrast as well.

2.2. Measurement in the (440) case

Due to the wavelength dependence in equation (3), the realizable $\delta\theta$ range is smaller in the (440) case. Therefore, in Fig. 6, only one pair of *Pendellösung* plateaus is visible. The slope of the phase is 11.5°/0.001 arcsec, which is consistent with the calculation and improves previous measurements (Springer *et al.*, 2010). This slope is steeper (approximately double) than in the (220) case; therefore, this case constitutes an extremely sensitive phase *versus* angle correlation (Zawisky, Springer & Lemmel, 2010).

The corresponding contrast is shown in Fig. 7. As in the (220), the visibility decreases fast. The different size of the error bars stems from different numbers of individual measurements per point.

Summarizing the measurement at the two Bragg peaks, the smaller wavelength yields a higher phase slope; however the beam deflection range is reduced. The resulting measured relationships and the calculations are in good agreement; however, the question of whether the accuracy of the measurements is sufficient for the determination of parameters like the scattering length will be discussed in the next section.

3. Systematic effects on the Laue phase

In this section different parameters are varied and we find that the Laue phase is strongly affected by the monochromator function, rocking angle and ρ-axis angle. The influence of the interferometer geometry is considered in the numerical calculations as well. In addition to the 'real' geometry, where the blade thickness varies slightly (2.940 ± 0.002 mm), calculations with the 'ideal' geometry are performed, where the thickness is constant for all interferometer blades (2.94 mm). Note that the fringe visibility at $\delta\theta = 0$ is, for the ideal interferometer, significantly higher due to equal blade thicknesses in both IFM paths. The change of the Laue phase will be evaluated particularly at the plateau positions indicated in Fig. 4.

3.1. Effect of various monochromator distribution functions

In the experiments a perfect crystal monochromator is used, with the theoretical Bragg curve given by equation (7), where I represents the intensity. The y–$\delta\theta$ relation is given in equation (2):

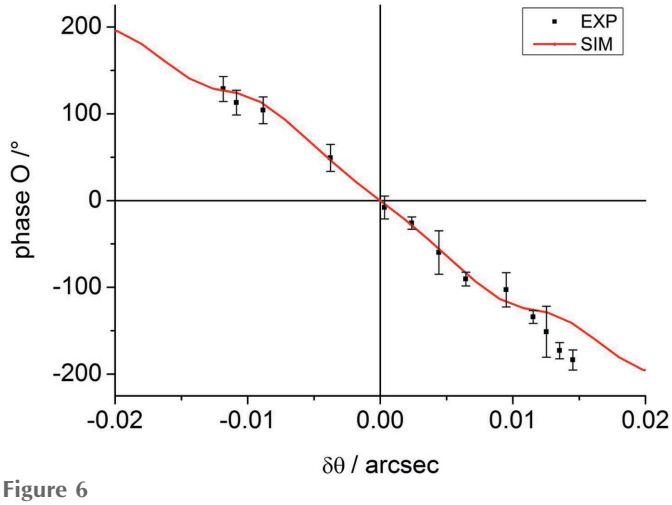

Figure 6
Measured and calculated Laue phase for the (440) case. The accessible $\delta\theta$ range shrinks, and the phase slope becomes steeper compared to (220).

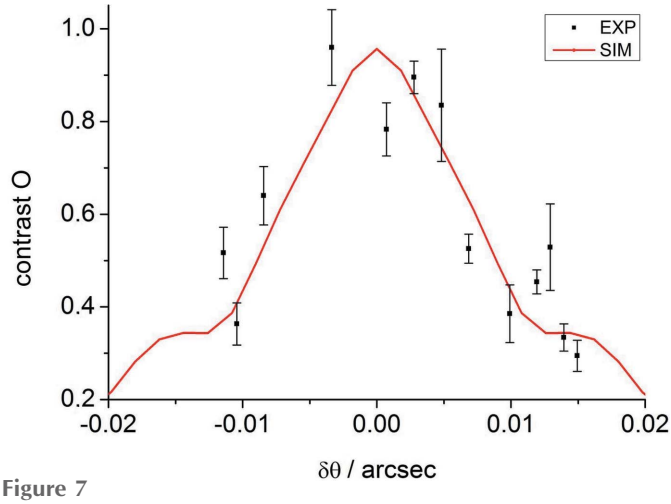

Figure 7
Measured and calculated contrast for the (440) case.

$$I = 1 \quad |y| < 1$$
$$I = 1 - (1 - y^{-2})^{1/2} \quad |y| > 1. \qquad (7)$$

In principle, one could also use a mosaic crystal monochromator. In order to study the differences we extended our simulations to the latter, represented by a Gaussian curve. Both curves are shown in Fig. 8.

Fig. 9 shows the remarkable effect of the monochromator functions on the Laue phase.

The difference in the phase calculated with a Bragg monochromator minus the phase calculated with a Gauss function depends strongly on the beam divergence σ_θ. This phase difference is caused by different excitations of plane-wave components that are slightly off-Bragg. The σ_θ value used is determined from a comparison with the rocking-curve measurement, which also depends on σ_θ. The best match is obtained for $\sigma_\theta = 1.6''$ (Fig. 12).

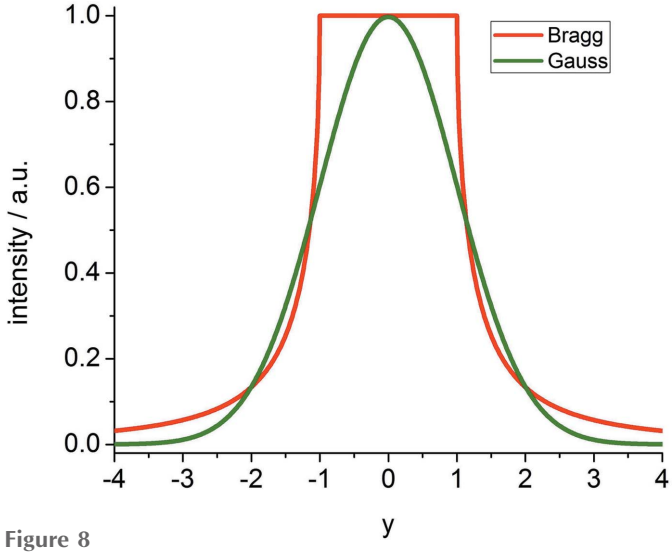

Figure 8
Comparison of Bragg and Gauss monochromator functions.

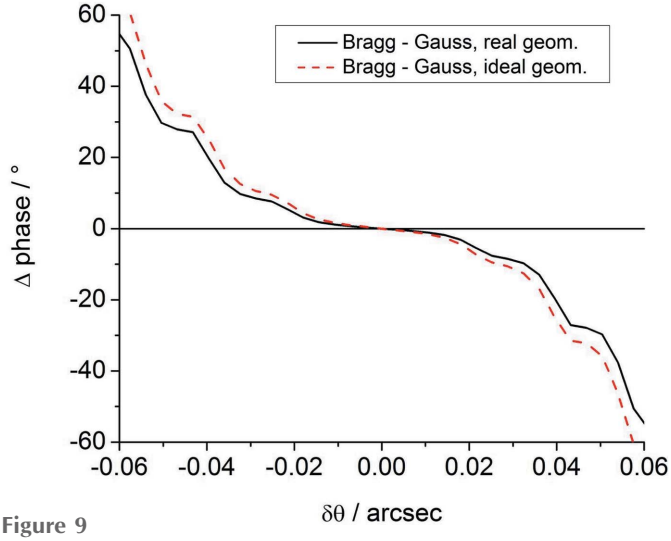

Figure 9
Simulation of the Laue phase difference (Bragg minus Gauss $\sigma_\theta = 1.6''$) *versus* the beam deflection $\delta\theta$ for the (220) case.

In the phase calculations the Bragg function with Darwin width equal to 1 is used because it is the physical monochromator function. However, in *IFMSIM*, it is possible to change the Darwin width of the Bragg curve and interpret it as the mosaicity of the monochromator, or the divergence of a single wavelength. The calculations are done for a single wavelength only since the wavelength dependence is negligible within our wavelength distribution of $\delta\lambda/\lambda \simeq 1.5\%$.

3.2. Effect of the monochromator mosaicity on the Laue phase

The beam divergence σ_θ for a single wavelength is determined by the mosaicity of the crystal monochromator. The tilt of the interferometer's lattice planes relative to the mono-

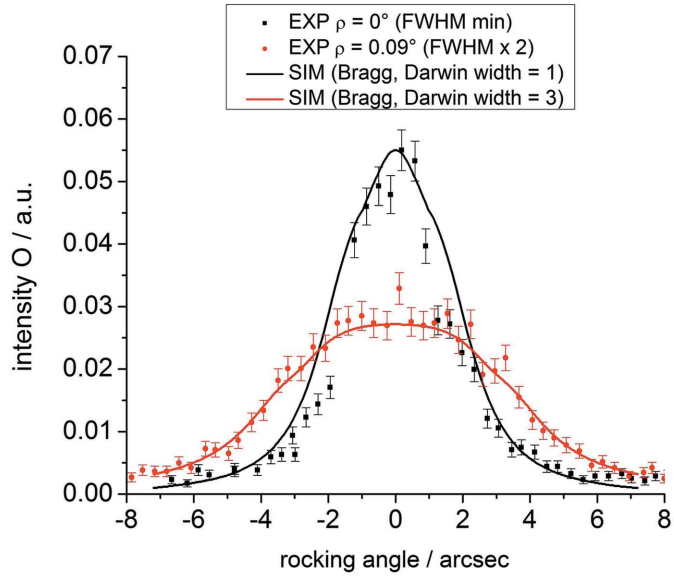

Figure 10
Rocking curves measured at various ρ-axis angles (beam divergences). The peak broadens with increasing tilt angle ρ.

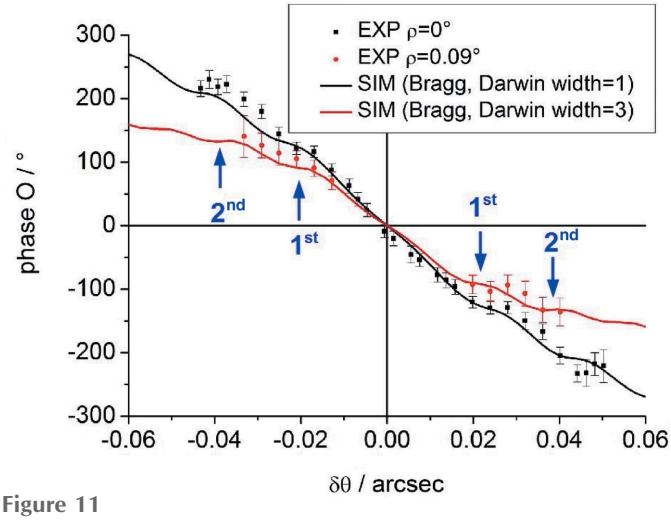

Figure 11
Laue phase for the (220) case at $\rho = 0°$ and $\rho = 0.09°$. The slope of the Laue phase decreases with increasing tilt. The labels '1st' and '2nd' indicate the positions of the *Pendellösung* plateaus.

chromator (ρ-axis angle, *cf.* Fig. 1*c*) increases the full width at half-maximum (FWHM) of the rocking curve and, thus, the effective mosaicity (Fig. 10). For large σ_θ (40″), the width of the rocking curve is so large that the intensity remains constant in the centre.

Fig. 11 compares the phase measurements for two different Darwin widths. The slope decreases with increasing Darwin width and approaches 4.3°/0.001 arcsec at a Darwin width >3. A larger Darwin width means that parts of the beam are further away from the Bragg condition of the interferometer crystal, where they contribute less and less to an average phase. This leads to a constant phase for Darwin width >3 at each $\delta\theta$ and therefore a fixed phase slope. The difference in the phase values at the marked $\delta\theta$ positions is remarkable (36–70°). The experimental data (rocking curve, Fig. 12) fit best to a Darwin width up to 1.2. The Laue phase difference between Darwin widths equal to 1 and 1.2 amounts to 6° for the first plateaus and 30° for the second.

3.3. Laue phase at different rocking positions

Because of experimental conditions, the angle between the interferometer and the neutron beam (rocking angle) can change slightly. The reasons for such drifts are mainly temperature changes within the setup (monochromator–interferometer–optical bench). Therefore, the effect of angular drift has to be studied by considering different rocking positions for the phase measurements. In Fig. 12, the investigated positions on the rocking curve are indicated.

These positions have been used to demonstrate the change in the Laue phase. The results are shown in Fig. 13. The slope of the phase reduces from 5.5°/0.001 arcsec at position 0 to 3°/0.001 arcsec at position ±B. It turns out that the difference in the phase values is surprisingly large (50–75°). In order to yield the phase uncertainty regarding the rocking angle we repeat the above phase measurement at the rocking position 0.18″, which is the accuracy of the used rocking rotation device. The mentioned temperature-caused drifts are avoided by resetting the rocking position very often between the phase measurements. The Laue phase changes by 1° (for the first plateaus) and 6° (for the second plateaus) relative to position 0. The phase change with the rocking-angle variation can be understood with the different phase averaging if the rocking position changes.

The corresponding contrast curve (Fig. 14) shows that the maximum is not at $\delta\theta = 0$, resulting from the combination of the rocking deviation and defocusing due to the different thick blades in the real geometry. This can be seen in the inset, where this situation is calculated for the ideal geometry.

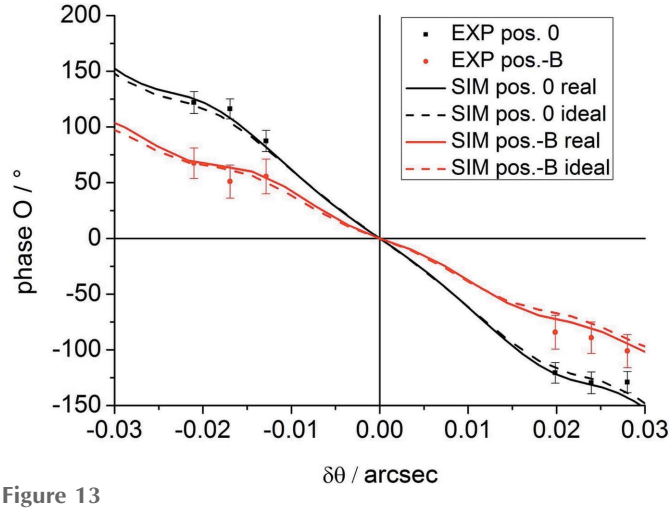

Figure 13
Laue phase at two different rocking positions for the (220) case. The slope depends strongly on the rocking angle.

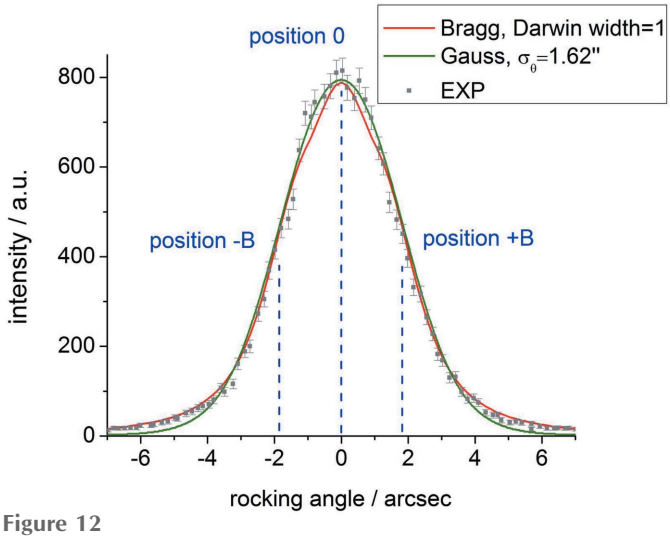

Figure 12
Experimental rocking curve compared with the theoretical one for the (220) case. Calculation with a Gauss monochromator with $\sigma_\theta = 1.62''$ fits as well as a Bragg curve with Darwin width equal to 1 to 1.2. The experimental positions on the rocking curve are −B, 0, +B with B = 1.8″.

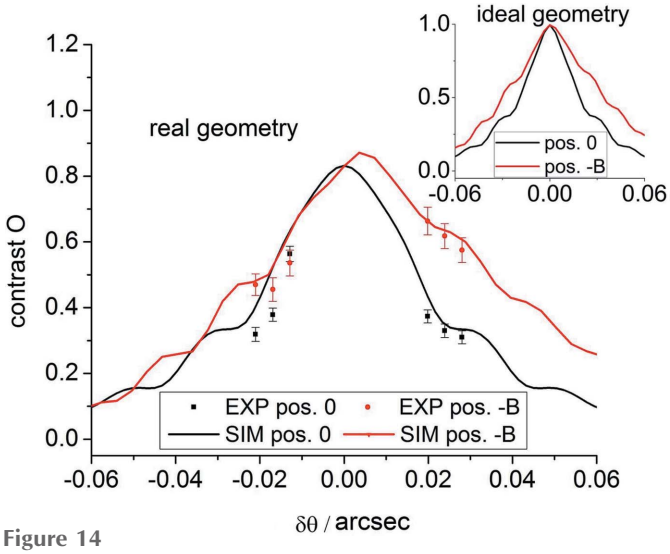

Figure 14
Contrast behaviour at two different rocking positions for the (220) case.

Table 1
Change of the Laue phase at the positions of the first and second plateaus, respectively, *cf.* Fig. 4 for the relevant parameter variations.

Calculation for the (220) Bragg function, Darwin width equal to 1 and real geometry.

Parameter	Variation	First plateaus	Second plateaus
IFM geometry	Ideal/real	4.7°	10.9°
Darwin width	1/1.2	6°	30°
Rocking angle	0.18″	1.5°	6°
Wavelength	0.03 Å	1°	6°
Prism angle β	0.001°	0.2°	0.4°
Prism angle ε	0.5°	0.75°	1°
Prism angle τ	1°	1°	2°
b_{ne} (440)	0.0003 fm	0.3°	(0.6°)
b_{ne} (220)	0.0003 fm	0.2°	0.45°

3.4. Additional parameters

The wavelength difference $\Delta\lambda$ between (220) and (440) changes the slope of the Laue phase from 5.5°/ 0.001 arcsec to 11.5°/ 0.001 arcsec, as already shown in §2. In addition, the slope depends strongly on the blade thickness D. A thicker sample increases the phase *versus* angle correlation (Zawisky, Springer & Lemmel, 2010). Furthermore, for thicker crystals the plateaus move closer to the centre; however, the contrast decreases more rapidly.

Moreover, the geometry of the prisms and their alignment has to be taken into account. In Table 1 the phase influence due to the alignment ε for all prisms, see Fig. 2, and a rotation in the x–y plane of all prisms (τ) are given.

A very fundamental parameter is the neutron–electron scattering length (Ioffe & Vrana, 2002), as contradicting values exist, *e.g.* Garching/Argonne: $b_{ne} = -0.00131$ (3) fm, Dubna: $b_{ne} = -0.00159$ (4) fm. The total scattering length comprises the precisely known nuclear scattering length b_{nuc} and the momentum-dependent electrostatic neutron–electron scattering contribution according to $b_{atom} = b_{nuc} + Z[1 - f(q)]b_{ne}$, where Z is the atomic number and $f(q)$ the electron form factor [references are summarized in Sparenberg & Leeb (2003)]. The values differ by $\Delta b_{ne} = 0.0003$ fm; two phase calculations with two such different b_{ne} values have been performed. The difference between these two phases is independent of the large value b_{nuc}, which is constant and the same in both cases. This Δb_{ne} difference would change the phase in our setup by 0.2° to 0.6° (Table 1); hence an experimental sensitivity of 0.1° would be required. Furthermore, the electron form factor changes the b_{ne} contribution with the wavelength, which makes the measurement at several Bragg peaks interesting. The table summarizes the influences of the different external and fundamental parameters.

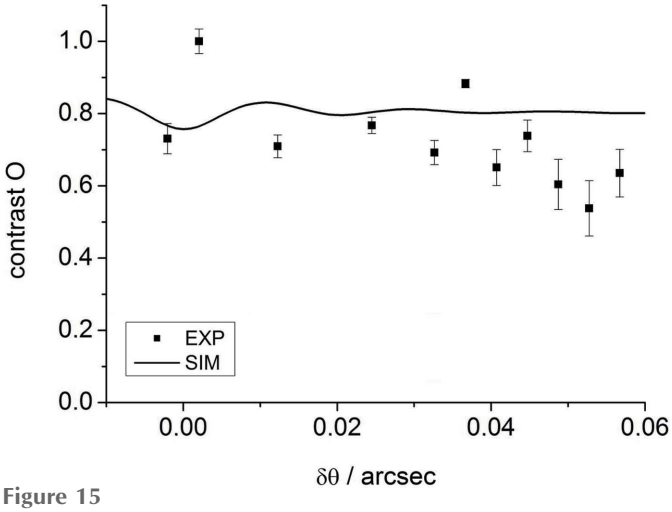

Figure 15
Maintaining the contrast with the 'relative phase method' [$\Delta\alpha = 1.1°$, $\delta\theta(220) = 0.0045''$].

4. Relative Laue method

To maintain the contrast at larger beam deflections, another method has been proposed (Springer *et al.*, 2010), where both prism pairs in Fig. 2 are deflecting the beam in front of blades 3 and 4, respectively; however, one prism has an additional offset angle $\Delta\alpha$. The advantage of the relative phase measurement is demonstrated in Fig. 15: the contrast remains constant even at larger deflection angles. For a further increase of $\delta\theta$, one can use prisms either with a larger β or scattering length density [equation (3)]. The phase sensitivity to b_{ne} increases with $\Delta\alpha$; however the phase change remains small (approximately 0.4°) for realistic offset angles and prism materials.

5. Conclusions

In this study, a large neutron interferometer was used to measure the phase shift of a perfect silicon crystal, in the vicinity of the Bragg condition (Laue phase). The rotation range of this crystal is $\delta\theta = \pm 0.06$ arcsec for the (220) and $\delta\theta = \pm 0.015$ arcsec for the (440) case. Distinct phase sensitivities of 5.5° (220) and 11.5° (440) per 0.001 arcsec deviation from the Bragg angle were achieved. Additional factors that affect this phase were identified and systematically investigated. With the setup used, two pairs of *Pendellösung* plateaus for the (220) case and one pair for the (440) case were identified. These plateaus are regions with increased sensitivity to fundamental parameters. The Laue phase was measured with an accuracy of ±9° (first plateaus) and ±15° (second plateaus). An additional temperature shielding of the whole monochromator–interferometer setup (currently planned at S18), as well as a more accurate rocking device would be necessary in order to increase the phase accuracy. To overcome the contrast reduction with increasing beam deflection, a relative measurement technique is presented.

Acknowledgements

We would like to thank the Austrian Science Foundation, project No. I530-N20, and the Collaboration Agreement between ILL and TU-Wien (ILL-1132.1-3) for financial support.

References

Authier, A. (2006). *Dynamical Theory of X-ray Diffraction.* Oxford University Press.

Bergmann, L. & Schaefer, C. (1993). *Experimentalphysik III.* Berlin: de Gruyter.

Graeff, W., Bauspiess, W., Bonse, U. & Rauch, H. (1978). *Acta Cryst.* A**34**, S238–S239.

Greene, G. & Gudkov, V. (2007). *Phys. Rev. C*, **75**, 015501.

Hirano, K. & Momose, A. (1996). *Phys. Rev. Lett.* **76**, 3735–3737.

Ioffe, A. & Vrana, M. (2002). *Appl. Phys. Mater. Sci. Process*, **74**, s314–s316.

Lemmel, H. (2007). *Phys. Rev. B*, **76**, 144305.

Lemmel, H. (2013*a*). *IFMSM – Simulation Software for Neutron Interfermometers*. Atominstitut Wien, Austria. http://www.ati.ac.at/~neutropt/experiments/software/.

Lemmel, H. (2013*b*). *Acta Cryst.* A**69**, 459–474.

Rauch, H. (1989). *Nucl. Instrum. Methods Phys. Res. Sect. A*, **284**, 156–160.

Rauch, H. & Petrascheck, D. (1974). *Grundlagen fuer ein Laue-Neutroneninterferometer.* Report AIAU 76401. Atominstitut der Oesterreichischen Universitaeten, Austria.

Rauch, H. & Werner, S. (2002). *Appl. Phys. A*, **74**, 314–316.

Shull, C. (1968). *Phys. Rev. Lett.* **21**, 1585–1589.

Sparenberg, J. & Leeb, H. (2003). *J. Electron Spectrosc. Relat. Phenom.* **129**, 315–317.

Springer, J., Zawisky, M., Lemmel, H. & Suda, M. (2010). *Acta Cryst.* A**66**, 17–21.

Wiedtfeldt, F., Huber, M., Black, T., Kaiser, H., Arif, M., Jacobson, D. & Werner, S. (2006). *Physica B*, **A74**, 385–386.

Zawisky, M., Springer, J., Farthofer, R. & Kuetgens, U. (2010). *Nucl. Instrum. Methods Phys. Res. Sect. A*, **612**, 338–344.

Zawisky, M., Springer, J. & Lemmel, H. (2010). *Nucl. Instrum. Methods Phys. Res. Sect. A*, **634**, S46–S49.